

A Dislocation Model for the Directional Anisotropy of Grain-Boundary Fracture

Glenn E. Beltz and Don M. Lipkin

Introduction

That fracture is governed by processes occurring over a wide range of length scales has been recognized since the earliest developments of modern fracture mechanics. Griffith's study of the strength of cracked solids^{1,2} is perhaps the earliest example of such multiscale thinking, pre-dating by several decades the first attempts to apply atomistically grounded traction-separation laws to fracture (e.g., the Orowan-Gilman model^{3,4}). Griffith recognized the critical condition for crack extension to be a statement of thermodynamic equilibrium of a cracked solid, representing a balance between the mechanical energy decrease upon crack extension and the corresponding increase in energy due to the newly created crack surface. Griffith determined the elastic strain energy of the cracked body using the continuum solution of the stress field about an ellipse⁵ and recognized that the potential energy associated with the cleavage surfaces of the crack was directly proportional to the surface energy, the latter deriving from the cohesive molecular forces of the solid. The Irwin-Orowan extension of Griffith mechanics to include plastic dissipation,⁶⁻⁹ which is known to occur on the mesoscopic length scale ($\sim 1-100 \mu\text{m}$), provides yet a further example of multiscale thinking in the early community of fracture researchers. In fact, the interaction of length scales is of central importance in most problems of fracture.

At first glance, it may seem that combining continuum and discrete (atomistic and/or dislocation) approaches to model fracture over a large range of length scales would be difficult to realize because of the significant differences in the domain sizes and characteristic constitutive properties

of the respective phenomena. However, such approaches have been successfully integrated by a number of investigators in recent years.¹⁰⁻²³ Presently, we provide an additional example of how discrete dislocation theories can be exploited to explain certain fracture phenomena in a way that links theories appropriate for vastly differing length scales.

Fracture Anisotropy: A Departure from Griffith Mechanics?

It is generally recognized that a material's intrinsic resistance to fracture need not be isotropic, depending on the crystallographic orientation of the fracture plane,^{24,25} as discussed in additional detail in the article by Gumbsch and Cannon in this issue. The anisotropy of brittle fracture is easily incorporated into Griffith fracture mechanics by allowing the surface energy γ_s to be a function of the crystallographic cleavage plane (see, for example, Reference 26). Upon further inspection, however, Griffith fracture mechanics appears to dictate that the resistance to fracture must be a scalar property and, as such, must not exhibit any anisotropy *within* a given cleavage plane. The fundamental measure of a material's resistance to brittle fracture—the work of cohesion of the solid (or the work of adhesion for interfacial fracture)—is, after all, path-independent. In other words, the fracture criterion is fully prescribed by the difference between the free energies of the initial state (i.e., the intact solid) and the final state (i.e., the two free surfaces). This conclusion is further supported by Rice's well-known implementation of the J -integral,^{27,28} whereby the fracture crite-

ri-
on is shown to be equal to the area under the traction-separation curve in the cohesive zone of the crack tip.

While it appears that the resistance to cleavage fracture should be constant once the crack is constrained to lie in a given fracture plane, some exceptions are known to occur. For instance, discrete interactions between the crack tip and the lattice lead to "lattice-trapping" effects^{25,29,30} and, therefore, to a deviation of the fracture resistance from the Griffith prediction. Recent experiments by Gumbsch and co-workers on tungsten single crystals²⁵ and atomistic simulations on tungsten and iron single crystals¹¹ have shown that lattice trapping can explain the seemingly anomalous dependence of the cleavage fracture resistance on the propagation direction. They considered cleavage in the [010] versus [011] directions on the (100) plane, as well as in the [100] versus [011] directions on the (011) plane. Differences in the orientation dependence of cleavage fracture resistance as large as $\sim 40\%$ were found, and in all cases, the fracture resistance exceeded the Griffith value. These effects were collectively ascribed to lattice trapping. Similar trends were found by Farkas in recent atomistic simulations of fracture along grain boundaries.³¹

Despite observations indicating that the fracture process exhibits crystallographic anisotropy, there is no methodology for predicting, let alone quantifying, such phenomena within the framework of continuum fracture mechanics. Presently, we revisit the assumption imposed by classical brittle-fracture mechanics that fracture along a prescribed plane must be path-independent. We consider the simple case of cleavage along a symmetrical tilt boundary and ask whether the crack resistance is affected by the direction of crack propagation. We show that path-independence is not a necessary condition in brittle-fracture mechanics and, in so doing, quantify the "polarity" of fracture along symmetrical tilt boundaries.

Dislocation Representation of Low-Angle Tilt Boundaries

The simplest kind of boundary that one can consider is the symmetrical tilt boundary, as depicted in Figure 1. A symmetrical tilt boundary can form when dislocations with Burgers vectors of magnitude b coalesce into a straight array, thus minimizing the total elastic energy in the system. If the angle of tilt is θ , and the dislocation spacing is p , then the kinematic constraint

$$\frac{p}{b} = \frac{\csc(\theta/2)}{2} \quad (1)$$

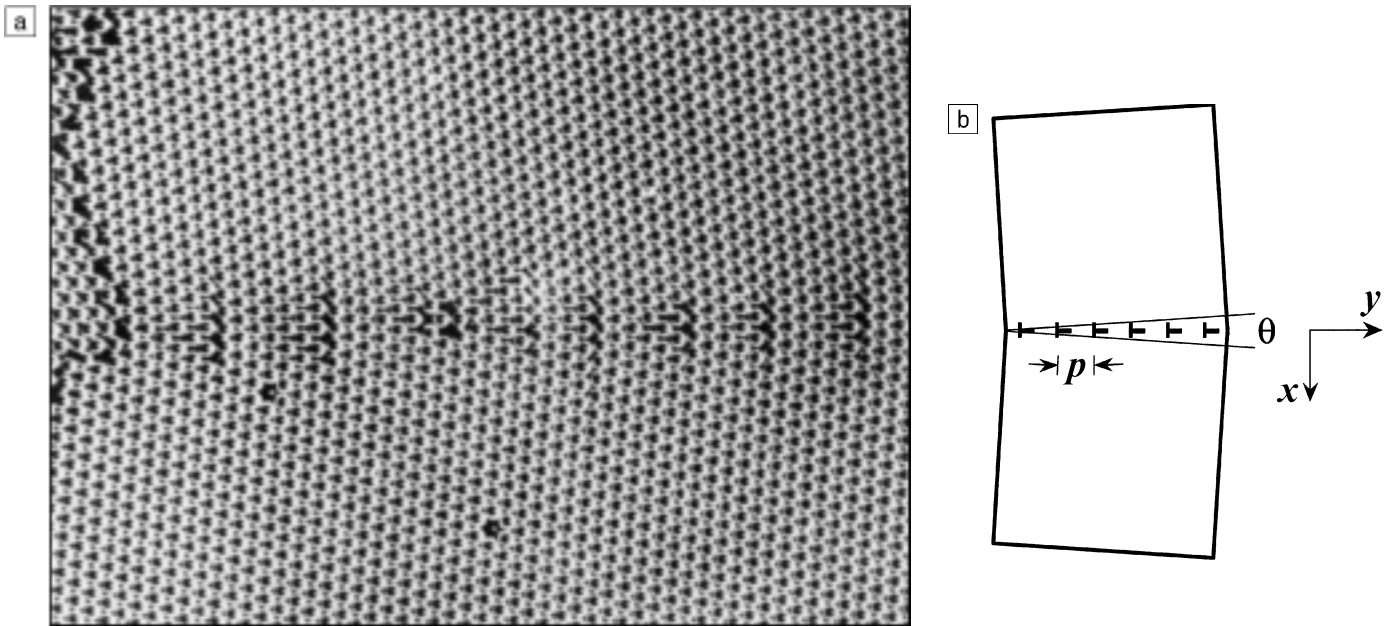


Figure 1. (a) A bubble-raft simulation of a low-angle tilt boundary, revealing that the boundary is comprised of a periodic array of edge dislocations (courtesy of P.G. Shewmon, Reference 42). (b) Schematic representation of a symmetrical tilt boundary having misorientation angle θ and comprising a dislocation periodicity p .

can be obtained by considering a right triangle, two sides of which have lengths given by b and p . Because the angles for which Equation 1 remains valid are small (e.g., when the dislocations are spaced as closely as five Burgers vectors, θ is $\sim 11.5^\circ$), the approximation $p/b = 1/\theta$, with θ expressed in radians, is commonly used. If the dislocations become too closely spaced—say, by less than a few Burgers vectors—the boundary is referred to as a *large-angle grain boundary*, and one must resort to more complex methods, such as atomistic simulation, for understanding these boundaries. An analogous representation can be made for the twist boundary, in which the adjacent grains are rotated with respect to one another about an axis that is normal to the boundary. In this case, the displacement (and stress) field can be represented by a cross-grid of screw dislocations. The most general boundaries, having mixed tilt and twist character, can be represented by a cross-grid of dislocations having both edge and screw character. A detailed discussion of how general low-angle grain boundaries are described using dislocation arrays may be found in the books by Nabarro,³² Hirth and Lothe,³³ and Hull and Bacon.³⁴ For ease of conceptualizing the problem of fracture along grain boundaries, we presently confine our attention to low-angle symmetrical tilt boundaries.

Barring internal stresses arising from thermal anisotropy or defect generation

during processing, individual grains in an unloaded solid can be approximated as stress-free. However, a single edge dislocation produces a stress field that, for an infinite, isotropic solid with shear modulus μ and Poisson's ratio ν , takes the form^{33,34}

$$\sigma_{xx} = -\frac{\mu by(3x^2 + y^2)}{2\pi(1 - \nu)(x^2 + y^2)^2}, \quad (2)$$

$$\sigma_{yy} = \frac{\mu by(x^2 - y^2)}{2\pi(1 - \nu)(x^2 + y^2)^2}, \quad (3)$$

and

$$\sigma_{xy} = \frac{\mu bx(x^2 - y^2)}{2\pi(1 - \nu)(x^2 + y^2)^2}. \quad (4)$$

The important feature to note about Equations 2–4 is that they indicate a relatively slow r^{-1} decay of stress, where $r \equiv (x^2 + y^2)^{1/2}$ represents the distance from the core of the dislocation. As the core of the dislocation is approached ($x, y \rightarrow 0$), Equations 2–4 predict an infinite stress. This issue is addressed in greater detail later in this article; suffice it to say for now that the stress equations are accurate only outside the “core region” of the dislocation ($r > r_0$), having a size of ~ 1 – 2 Burgers vectors. Inside the core, the constitutive response of the solid is highly nonlinear, and the stresses are, as would be expected, bounded.

When considering a tilt boundary, it is necessary to sum the stress field arising from an infinite number of dislocations lying on the y axis and spaced apart by a distance p . These sums are defined and analytically simplified by Hirth and Lothe,³³ and we will not reproduce the expressions here. We note, however, that the stresses decay *exponentially* with distance away from the array (Figure 2a shows the shear-stress component $\tau = \sigma_{xy}$), in contrast to the sluggish $1/r$ stress field for the single dislocation. Hence the stress due to the array decays practically to zero over a distance of the dislocation spacing, indicating the absence of a long-range stress field—a fundamental property of grain boundaries. In the plane of the array, the stress field takes on an oscillatory nature with periodicity p . Figure 2b shows the normal stress $\sigma = \sigma_{xx}$ for $y = 0$ (i.e., within the array). At the midpoint between two dislocations, this stress component vanishes. At distances much less than p from any given dislocation, the stress field of the array can be shown to approach that of the individual dislocation.

Brittle Fracture

We now turn our attention to cracks. Upon loading, the stress field of a cracked solid asymptotically takes the form $1/\sqrt{r}$, where r is the distance from the tip. This is true near *any* crack tip, regardless of other geometric features of the system. Thus for

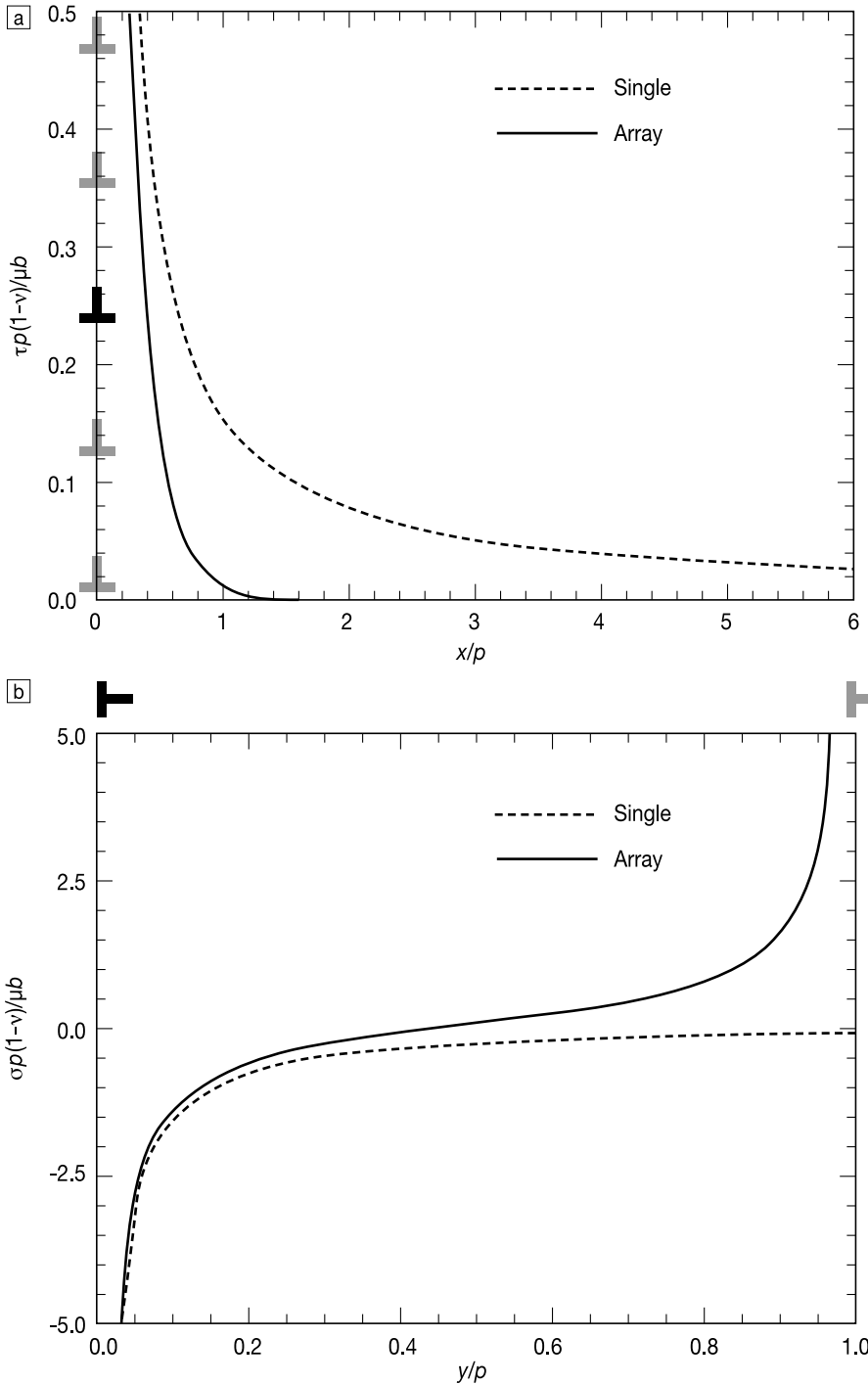


Figure 2. Comparison of stresses due to a low-angle tilt boundary (solid line) and an isolated dislocation (dashed line). The shear stress moving away from the boundary is given in (a), while the normal stress σ_{xx} within the boundary is given in (b). Note the rapid decay of τ associated with the boundary as compared with that of the single dislocation.

a given geometry and loading, the stress components can be written as

$$\sigma_{ij} = \frac{K f_{ij}(\theta)}{\sqrt{2\pi r}} \quad (5)$$

where the angular functions $f_{ij}(\theta)$ can be determined, given the loading configuration, and K represents the “intensity” of the stress singularity and is commonly known as the *stress intensity factor*. For con-

venience, we will restrict the discussion to “Mode I” loading, wherein the crack is symmetrically loaded about the crack plane, giving rise to crack opening or closure. K scales linearly with the magnitude of external loading and depends (sometimes in a complex way) on the geometry of the system. As a simple example, for a through-crack of length $2a$, centered on the origin of an infinite solid and subject to remote tension σ_∞ oriented normal to the crack plane, $K = \sigma_\infty \sqrt{\pi a}$. Note that in the absence of external loading, $K = 0$, and the crack has no driving force for extension. Another significant feature of K is that it is related to the elastic energy-release rate G (change of total elastic energy stored in the system, including the potential stored in the loading system, per unit area of crack advance) through the Irwin relation $G = (1 - \nu)K^2/2\mu$. The classical Griffith criterion for fracture may then be expressed as $G = G_c$; that is, when the “applied” G achieves a certain threshold value, the crack propagates. Due to the monotonic relation between G and K , the stress-intensity factor may be directly used in the fracture criterion such that the critical stress-intensity factor required for fracture is given by

$$K_G = \sqrt{\frac{2\mu G_c}{1-\nu}} \quad (6)$$

Crack/Dislocation Interactions

Because a dislocation is a source of stress, it can induce an additional stress-intensity factor, designated K_D , on a crack. The simplest case is a semi-infinite crack having an edge dislocation on the prolongation of the crack plane, as depicted in Figure 3a. The stress-intensity factor for this geometry was given by Thomson:³⁵

$$K_D = \frac{\mu b}{(1-\nu)\sqrt{2\pi s}} \quad (7)$$

where s is the distance from the crack tip to the dislocation. Note that K_D diverges as the crack tip approaches the dislocation.

What happens when a relatively long crack is introduced onto a tilt boundary? At first glance, it appears logical to com-

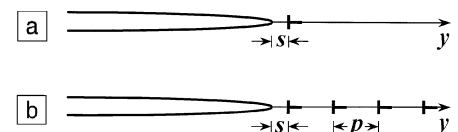


Figure 3. A semi-infinite crack on a boundary containing (a) a single dislocation and (b) a dislocation array.

pute the summation of the stress-intensity factor of Equation 7 over each dislocation in the array ahead of the crack, as indicated schematically in Figure 3b. The resulting stress-intensity factor should depend not only on the dislocation spacing p , but also on the distance s of the first dislocation to the crack tip:

$$K_D = \frac{\mu b}{(1-\nu)\sqrt{2\pi}} \sum_{n=0}^{\infty} \frac{1}{\sqrt{s+np}}. \quad (8)$$

Inspection of Equation 8 reveals that the series is divergent! This result would imply that a crack located on a tilt boundary is unstable with respect to fracture (or healing, depending on the orientation of the crack with respect to the array). This conclusion is, of course, unphysical. The problem with the simplistic approach leading to Equation 8 stems from the fact that dislocations previously comprising the boundary (to the left of the tip in Figure 3b), which are presumably annihilated as the crack propagates, still exert a force on the crack tip.

To understand the effect of these so-called image, or virtual, dislocations, we first consider the general problem of a dislocation introduced into a body containing an arbitrarily shaped hole (Figure 4) in an infinite, two-dimensional solid. Imagine introducing the dislocation at point B by creating an imaginary cut along the ray

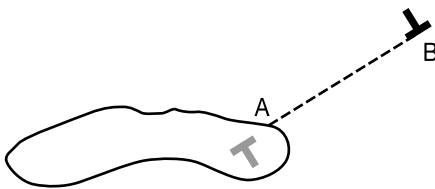


Figure 4. There are two distinct approaches to introducing a dislocation at location B near an arbitrarily shaped hole. In the first, the dislocation is injected from the hole by making a cut from the surface of the hole (location A) to B and shearing the opposing faces across the slip plane AB by the Burgers vector. Alternatively, the dislocation can be introduced from an exterior surface of the body (location C, not shown) by making a cut between C and B, then shearing the opposing faces across the slip plane BC by the Burgers vector. The first method results in no net Burgers vector, indicating the creation of an image dislocation within the hole having an opposite-signed Burgers vector. The second method does not lead to the creation of an image dislocation. The two constructions lead to unique stress fields.

AB, then displacing the faces of AB by the appropriate Burgers vector. In this case, there are actually *two* dislocations in the system: one is the primary dislocation at point B, and the other is the residual dislocation represented by the hole itself. A Burgers circuit around point B results in the expected Burgers vector \mathbf{b} ; applying the circuit to the hole results in a Burgers vector of $-\mathbf{b}$, that is, the hole contains one negative virtual dislocation. Drawing the circuit around the entire hole/dislocation pair gives a null Burgers vector, because in fact a dislocation dipole has been introduced into the system. If we now consider introducing the dislocation at B via an imaginary cut that runs from point B to a point on the *external* boundary of the body (albeit an infinite distance away), and displacing the faces of this cut by the Burgers vector, we again have a dislocation of Burgers vector \mathbf{b} at B; however, the Burgers circuit around the hole yields a null Burgers vector (i.e., the hole contains no virtual dislocations). This distinction has no relevance to the semi-infinitely long crack represented in Figure 3, since the crack faces themselves constitute part of the external boundary of the solid and no additional crack-tip force is created. However, for the case of an internal crack, the creation or annihilation of dislocations has the direct consequence of modifying the crack-tip stress intensity. For the special case of an elliptical hole, the stress field resulting from such virtual dislocations has been worked out by Kratochvíl³⁶ and Hirth.³⁷

In general, then, a finite crack of length $2a$ may contain an arbitrary number of virtual dislocations, each inducing a force on the crack tip. The stress-intensity factor K_d , induced by a virtual dislocation on the right-hand crack tip, was independently calculated by Lin and Hirth³⁸ and Zhang and Li:³⁹

$$K_d = \frac{-\mu b}{2(1-\nu)\sqrt{\pi a}}. \quad (9)$$

Note that Equation 9 does not depend on the location of the virtual dislocation within the crack. Similarly, the stress-intensity factor due to a real dislocation lying in the crack plane ahead of the right-hand tip of a finite crack of length $2a$ is given by³⁹

$$K_D = \frac{\mu b}{2(1-\nu)\sqrt{\pi a}} \left(\sqrt{\frac{2a+s}{s}} - 1 \right). \quad (10)$$

Note that Equation 10 reduces to Equation 7 in the limit as $a \rightarrow \infty$.

Grain-Boundary Fracture

We now imagine an infinitely long, crack-free, low-angle tilt boundary. At some point along the boundary (without loss of generality, we can define this point as the origin), a crack nucleates and is forced to extend in either direction along the boundary (see Figure 5). As the crack extends, real dislocations are converted into virtual dislocations. The number of dislocations that are annihilated and that become virtual dislocations, m , increases stepwise as the crack grows and, for $a/p \gg 1$, can be thought of as a continuous and linear function of a such that $m \approx 2a/p$. The total stress-intensity factor induced by the dislocations on the right-hand crack tip, K_{gb}^+ , is calculated by summing Equation 10 over all remaining dislocations on the boundary (to the left and right of the crack tip), then adding Equation 9 for all m virtual dislocations annihilated by the crack:

$$K_{gb}^+ = \frac{\mu b}{2(1-\nu)\sqrt{\pi a}} \times \left\{ \sum_{n=0}^{\infty} \left[\left(\sqrt{\frac{2a+s+np}{s+np}} - 1 \right) + \left(\sqrt{\frac{s+np}{2a+s+np}} - 1 \right) \right] - \frac{2a}{p} \right\}. \quad (11)$$

The first two terms in the summation represent the shielding K_D from all real grain-boundary dislocations to the right of the right-hand tip ($y > a$) and to the left of the left-hand tip ($y < -a$), respectively. The last term represents the shielding K_d from all virtual dislocations annihilated by the crack ($-a < y < a$). In the limit $a \rightarrow \infty$, both terms within the square brackets of Equation 11 diverge, as was the case with Equation 8. However, the term due to the image dislocations within the crack, which itself diverges as $a \rightarrow \infty$, keeps Equation 11 convergent.

With no apparent analytic simplification of Equation 11, we must resort to numerical evaluation. Selecting appropriate normalization factors and taking the limit $a \rightarrow \infty$, we arrive at a single curve for K induced at the crack tip of a forward-propagating, semi-infinite crack as a function of relative crack-tip position between two dislocations (Figure 6). Starting immediately to the right of the origin ($\Delta a/p \rightarrow 0^+$), a dislocation has just been annihilated, and a full periodic distance p remains to the next real dislocation. At this point, the crack actually experiences shielding from the grain-boundary dislocations, as evidenced by a negative

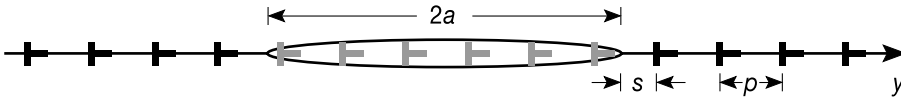


Figure 5. The stress field associated with a finite crack on a low-angle grain boundary can be regarded as the superposition of the stresses associated with individual dislocations. Image dislocations, occupying positions where the crack has extended, must be included in this calculation.

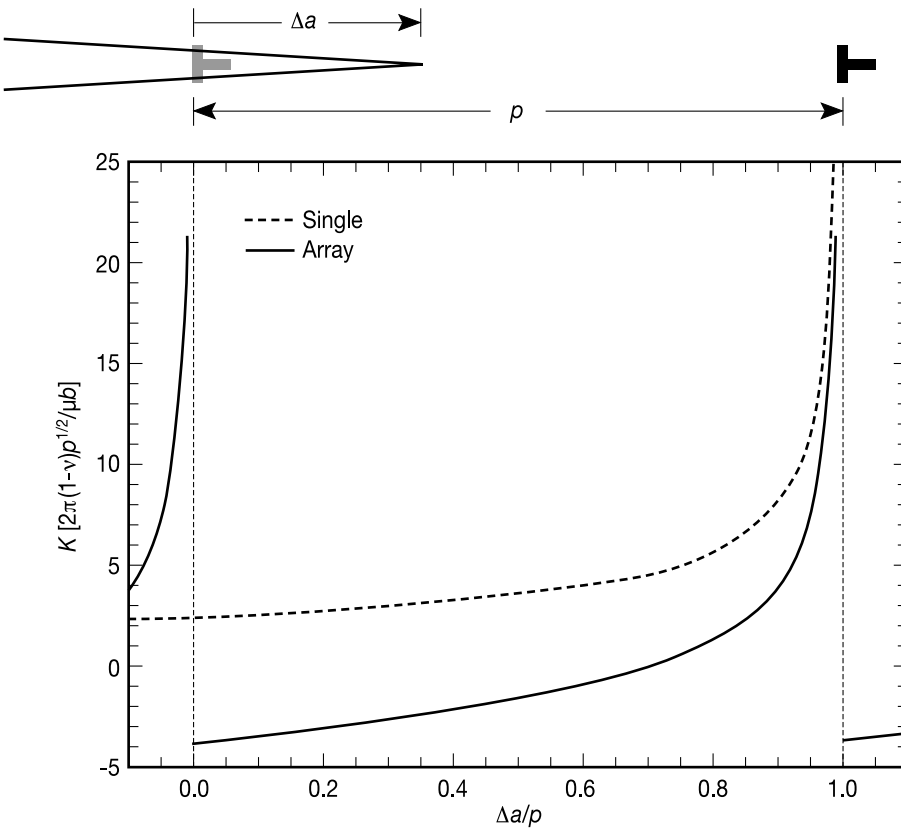


Figure 6. Stress-intensity factor K_{gb}^+ induced on the forward-propagating crack tip due solely to the dislocation array. The crack is taken as sufficiently long to allow a periodic function to develop.

stress-intensity factor. Under an applied load characterized by K_a , the net stress-intensity factor at the crack tip is $K_{tip}^+ = K_a + K_{gb}^+$, where K_{gb}^+ is given by Equation 11. The threshold condition for crack extension is attained when K_{tip}^+ reaches the Griffith fracture limit K_C . To propagate the crack tip along the boundary, K_a must be sufficiently large so that K_{tip}^+ overcomes the maximum shielding along the entire interval p between adjacent dislocations. As is evident from Figure 6, the maximum shielding for propagation in the forward direction occurs at $\Delta a/p \rightarrow 0^+$. Therefore, the critical applied stress intensity for crack propaga-

tion in the forward direction, defined as $K_a \rightarrow K_c^+$, is:

$$K_c^+ \approx K_C + 3.6 \frac{\mu b}{2\pi(1-\nu)\sqrt{p}} \quad (12)$$

Thus, the *apparent*, or “applied,” stress-intensity factor necessary to maintain crack extension is greater than the Griffith value by an amount that is inversely proportional to the spacing of dislocations comprising the grain boundary. As the angle of grain-boundary tilt diminishes, $p \rightarrow \infty$, and the classical Griffith result is recovered. It should be noted that K_C , as given in Equation 12, represents the Grif-

fith value of the *grain-boundary* fracture resistance and is therefore a function of the tilt angle. K_C can be related to the surface energy of the solid via the Dupré relation $G_C = 2\gamma_s(\theta) - \gamma_{gb}(\theta)$ and the Irwin relation (Equation 6).

We now consider propagation of a semi-infinite grain-boundary crack in the reverse direction. The only distinction from the forward-propagating crack is that it experiences the effect of dislocations having opposite-signed Burgers vectors. Therefore, the stress-intensity factor induced by the array of dislocations is simply the negative of that given by Equation 11 and Figure 6: $K_{gb}^- = -K_{gb}^+$. If the crack were to propagate in this direction, the greatest crack-tip shielding occurs when the tip just approaches a dislocation (this is analogous to position $\Delta a/p \rightarrow 0^-$ in Figure 6). At this location, an infinitely large applied K_a would appear to be necessary to overcome the nominally unbounded shielding induced by the dislocation, such that $K_c^- \rightarrow \infty$. This conclusion reveals one of the major deficiencies of continuum elastic dislocation theory: the crack *must* be able to penetrate through the core region of the dislocation with a finite resistance. Atomistic methods, such as those discussed elsewhere in this issue, are clearly the preferred way to treat the mechanics of extremely close or overlapping crack/dislocation cores. However, we can make a reasonable first-order estimate of the reverse-fracture criterion using a core-cutoff approach.

We conjecture that as the crack approaches the dislocation, the dislocation core slightly redistributes itself over its slip plane. In so doing, no singularity in the crack-tip stress intensity arises. As the crack passes through the core, the slip discontinuity that defines the dislocation recedes into the free surfaces of the crack wake. This conceptual model is, in a sense, just the opposite of the dislocation-nucleation process described by Rice.¹² We have carried out a preliminary study of this mechanism using the Peierls-Nabarro^{40,41} model of the dislocation core. Details of the implementation of the model and of the subsequent results are outside the scope of the present discussion. However, we note that a good empirical fit to the results is obtained when the stress-intensity factor given by (the negative of) Equation 11 is evaluated at a crack-tip/dislocation spacing of approximately one Burgers vector. The latter length scale defines the dislocation core-cutoff parameter r_0 .

Evaluating Equation 11 in the limit as $a \rightarrow \infty$, the threshold condition for fracture in the reverse direction occurs when K_{tip}^-

at the location of maximum shielding along the entire interval p between adjacent dislocations reaches K_C . This criterion corresponds to a critical applied stress intensity K_C^- :

$$K_C^- \approx K_C + \frac{\mu b}{(1 - \nu)\sqrt{2\pi r_0}} - 3.6 \frac{\mu b}{2\pi(1 - \nu)\sqrt{p}}, \quad (13)$$

where the second term corresponds to the stress intensity induced by the lead dislocation, and the last term is the stress intensity induced on the crack tip by the remainder of the array of real and virtual dislocations. Note that the value of K_C^- , as given by Equation 13, is finite.

Implications and Directions for Future Investigation

We set out to determine whether the directional anisotropy of cleavage fracture along a tilt boundary can be predicted—and quantified—using a simple extension of the Griffith theory to include trapping at geometrically necessary (i.e., nonredundant) grain-boundary dislocations. We arrived at two unique expressions for the fracture resistance along a grain boundary: Equation 12 for the resistance to fracture in the “antishielding” direction and Equation 13 for the analogous resistance in the “shielding” direction. It is worthwhile to estimate the magnitude of the predicted anisotropy for a low-angle grain boundary in a representative metallic solid. For this illustration, we consider: $\mu = 100$ GPa, $\nu = 0.3$, and $b = r_0 = 3$ Å. Assuming a grain-boundary tilt angle of $\sim 5^\circ$, Equation 1 gives $p/b \sim 11.5$. Substituting these values into Equations 12 and 13, one obtains $K_C^+ = K_C + 0.4$ MPa \sqrt{m} and $K_C^- = K_C + 0.6$ MPa \sqrt{m} for the antishielding and shielding directions, respectively, where the typical grain-boundary toughness of a Griffith solid may be estimated as $K_C = 0.5$ MPa \sqrt{m} . From this estimate, we conclude that (1) the interaction between a grain-boundary crack and the nonredundant grain-boundary dislocations leads to an intrinsic toughness that is roughly two times greater than the limiting Griffith value, and (2) there is an appreciable and heretofore unquantified directional anisotropy ($\sim 20\%$) in the grain-boundary fracture resistance. The magnitude of the present results is, of course, dependent on the magnitude of the parameters chosen for the calculations.

A number of issues remain to be resolved in extending the present treatment

to a more general description of the directional anisotropy of crystalline fracture. The present model does not account for the development toward a mature crack, the behavior of which is often dominated by larger-scale processes such as the development of a plastic zone, the presence of multiple grains, and various effects of other heterogeneities (such as second-phase particles). The motion of surrounding dislocations in the crystal is not accounted for in this treatment, nor is dislocation nucleation. The shielding effect of previously emitted dislocations can substantially reduce the local stress field around the crack and therefore increase the critical applied loads for dislocation nucleation and cleavage. Although emitted dislocations are assumed to be swept sufficiently far away that we may ignore these shielding effects, background dislocations and plastic dissipation have been shown to play a critical role in the applied loads necessary to maintain the “local” loads described in this article.^{6–9,18–20} These effects are expected to influence the fracture behavior in a highly nonlinear fashion (sometimes referred to as the “valve” effect) and can account for an increase in the applied loads by up to three to four orders of magnitude from the loads discussed in the present work.²⁰ Perhaps most important is the fact that the valve effect can induce profound changes in the macroscopic behavior of real solids for what appear to be modest changes in the Griffith criterion. We leave such considerations for future investigation.

Acknowledgments

This work was partially supported by the MRL Program of the U.S. National Science Foundation under Award No. DMR96-32716. We would like to thank Diana Farkas, Peter Gumbsch, and Paul Follansbee for useful discussions and Paul Shewmon for permission to reproduce the image for Figure 1a.

References

1. A.A. Griffith, *Philos. Trans. R. Soc. London, Ser. A* **221** (1921) p. 163.
2. A.A. Griffith, in *Proc. 1st Int. Cong. on Applied Mechanics*, edited by C.B. Biezeno and J.M. Burgers (J. Waltman Jr., Delft, Netherlands, 1924) p. 55.
3. E. Orowan, *Rep. Progr. Phys.* **12** (1949) p. 48.
4. J.J. Gilman, *J. Appl. Phys.* **31** (1960) p. 2208.
5. C.E. Inglis, *Proc. Inst. Naval Architects* **55** (1913) p. 219.
6. E. Orowan, *Trans. Inst. Engrs. Shipbuilder Scot.* **89** (1945) p. 165.
7. J.R. Rice, in *Proc. 1st Int. Conf. on Fracture*, edited by T. Yokobori, T. Kawasaki, and J.L. Swedlow (Japanese Society for Strength and

- Fracture of Materials, Tokyo, Japan, 1966) p. 309.
8. E.D. Hondros and M.P. Seah, *Int. Metal. Rev.* **222** (1977) p. 262.
9. R. Thomson, *J. Mater. Sci.* **13** (1978) p. 128.
10. J. Frenkel, *Z. Phys.* **37** (1929) p. 572.
11. S. Kohlhoff, P. Gumbsch, and H.F. Fischmeister, *Philos. Mag. A* **64** (4) (1991) p. 851.
12. J.R. Rice, *J. Mech. Phys. Solids* **40** (1992) p. 239.
13. Y. Sun, G.E. Beltz, and J.R. Rice, *Mater. Sci. Eng., A* **72** (1993) p. 67.
14. W. Yang, H. Tan, and T. Guo, *Modell. Simul. Mater. Sci. Eng.* **2** (3A) (1994) p. 767.
15. G.E. Beltz and L.B. Freund, *Philos. Mag. A* **69** (1994) p. 183.
16. G. Xu, A.S. Argon, and M. Ortiz, *Philos. Mag. A* **72** (2) (1995) p. 415.
17. G. Xu, A.S. Argon, and M. Ortiz, *Philos. Mag. A* **75** (2) (1997) p. 341.
18. G.E. Beltz, J.R. Rice, C.F. Shih, and L. Xia, *Acta Mater.* **44** (10) (1996) p. 3943.
19. D.M. Lipkin and G.E. Beltz, *Acta Mater.* **44** (4) (1996) p. 1287.
20. D.M. Lipkin, D.R. Clarke, and G.E. Beltz, *Acta Mater.* **44** (10) (1996) p. 4051.
21. R. Miller, R. Phillips, G.E. Beltz, and M. Ortiz, *J. Mech. Phys. Solids* **46** (1998) p. 1845.
22. G.E. Beltz, D.M. Lipkin, and L.L. Fischer, *Phys. Rev. Lett.* **82** (1999) p. 4468.
23. G.E. Beltz and L.L. Fischer, *Philos. Mag. A* **79** (6) (1999) p. 1367.
24. J.-S. Wang and P.M. Anderson, *Acta Metall. Mater.* **39** (5) (1991) p. 779.
25. J. Riedle, P. Gumbsch, and H.F. Fischmeister, *Phys. Rev. Lett.* **76** (19) (1996) p. 3594.
26. C. Herring, in *Structure and Properties of Solid Surfaces*, edited by R. Gomer and C.S. Smith (University of Chicago Press, Chicago, 1953) p. 5.
27. J.R. Rice, in *Fracture: An Advanced Treatise*, Vol. 2, edited by H. Liebowitz (Academic Press, New York, 1968) p. 191.
28. J.R. Rice, *J. Appl. Mech.* **35** (1968) p. 379.
29. R. Thomson, C. Hsieh, and V. Rana, *J. Appl. Phys.* **42** (8) (1971) p. 3154.
30. E.R. Fuller Jr. and R. Thomson, in *Proc. 4th Int. Conf. on Fracture*, Vol. 3, edited by D.M.R. Taplin (Pergamon Press, Oxford, 1978) p. 387.
31. D. Farkas, *Philos. Mag. Lett.* **80** (4) (2000) p. 229.
32. F.R.N. Nabarro, *Theory of Crystal Dislocations* (Clarendon Press, Oxford, 1967).
33. J.P. Hirth and J. Lothe, *Theory of Dislocations*, 2nd ed. (John Wiley & Sons, New York, 1982).
34. D. Hull and D.J. Bacon, *Introduction to Dislocations*, 3rd ed. (Pergamon Press, New York, 1984).
35. R. Thomson, in *Solid State Physics*, edited by H. Ehrenreich and D. Turnbull (Academic Press, New York, 1986) p. 1.
36. J. Kratochvíl, *Czech. J. Phys. B* **11** (1961) p. 324.
37. J.P. Hirth, *Acta Mater.* **47** (1) (1999) p. 1.
38. I.-H. Lin and J.P. Hirth, *Philos. Mag. A* **50** (6) (1984) p. L43.
39. T.-Y. Zhang and J.C.M. Li, *Acta Metall. Mater.* **39** (11) (1991) p. 2739.
40. R.E. Peierls, *Proc. Phys. Soc.* **52** (1940) p. 23.
41. F.R.N. Nabarro, *Proc. Phys. Soc., London* **59** (1947) p. 256.
42. P.G. Shewmon, *Transformations in Metals* (J. Williams, Jenks, OK, 1983) p. 26. □